doi:10.1038/nature11205

1. DATA COMPILATIONS

Measurements of ecosystem respiration were compiled for nine different ecosystem types –forested ecosystems, non-forested terrestrial ecosystems, soils, estuarine pelagic zones, estuarine benthic zones, lake pelagic zones, lake benthic zones, rivers, and oceans – to construct a global database. Our study uses two types of data: daily fluxes for the "short-term" analyses (see Section 5 below), and annual fluxes for the "long-term" analyses (see Section 6 below). Where possible, we have made these data available here (Online Appendix 1). Data from FluxNet (http://www.fluxnet.ornl.gov) and GLEON (http://www.gleon.org/) could not be made available because these global synthesis networks require prior arrangement for data access (see Tables S1.1 and S1.2 below). Analyses of short-term data were conducted using *in-situ* estimates of respiration and temperature; only fluxes at temperatures above 0°C were considered (see section 5 below for an explanation). Analyses of long-term data were conducted using annually integrated estimates of respiration, which were calculated from the daily measurements (see below). Sites with measurements spanning a time period of < 8 months (240 days) were excluded from the long-term analyses, regardless of the resolution of the data, to avoid potential biases.

With the exception of the FluxNet database, which was used for the forest and non-forest ecosystem analyses, in some instances, there was temporal variation in sampling effort (e.g. fewer measurements were sometimes taken during colder months). Annual estimates were therefore obtained by first linearly interpolating the data over an entire year to obtain 365 daily estimates of respiration and temperature, an approach commonly used in broad-scale comparative studies, e.g. Ref. 1. Annual respiration was then calculated as the sum of the 365 daily estimates. If measurements spanned more than one year, measurements were averaged (if necessary) to obtain a

single estimate for each of the 365 days, e.g. measurements taken on January 1, 2000 and January 1, 2001 would be averaged to obtain an estimate for day 1. If measurements were not taken on day 1 (January 1) or 365 (December 31), measurements from the earliest and latest calendar day of the year were repeated outside of the 1-to-365 day range to facilitate interpolation. For example, if the first estimate was obtained on January 2 and the last estimate was obtained on December 28, the January 2 estimate was assigned to days 2 and 367, and the December 28 estimate was assigned to days 362 and -3.

Forested and non-forested terrestrial ecosystems

The short- and long-term analyses of forested and non-forested terrestrial ecosystems were conducted using data from the La Thuile FluxNet database (www.fluxdata.org), which is comprised of night-time net CO_2 flux estimates for every day of the year using the eddy-covariance technique. We analysed data for 52 of the 60 sites in the analysis of Mahecha *et al.*[2]. The other 8 sites were excluded because they were severely affected by drought, resulting in an inverse relationship between respiration and temperature (see Figure S1.1 below). These 8 sites include Amazon rainforest[3,4], Mediterranean grassland[5], Californian scrubland[6], and Californian savannah grassland[7,8]. Data were subjected to quality-control checks described by Papale *et al.*[9]. We separately analysed respiration data for forest ecosystems (38 sites) – deciduous broadleaf forests, evergreen broadleaf forests, and evergreen needle-leaf forests combined – and non-forest ecosystems (14 sites) – croplands, shrublands, grasslands, savannahs and woody savannahs – because of potential differences in the importance of factors other than temperature on the temperature dependence of flux.

For the analyses of long-term data, we included the full series of temperature

and respiration measurements (including gap-filled estimates). For the analyses of short-term data, we excluded flux estimates obtained by gap filling. We also excluded respiration measurements taken at air temperatures < 0°C because, at such temperatures, ecosystem respiration occurs primarily in soil horizons that remain above freezing[10]. Thus, at air temperatures < 0°C, air temperatures may not accurately reflect the thermal environment where ecosystem respiration is occurring[10], particularly if the soil is insulated by snow[11]. For the aquatic data, temperatures always exceeded 0°C, so this issue was not applicable.

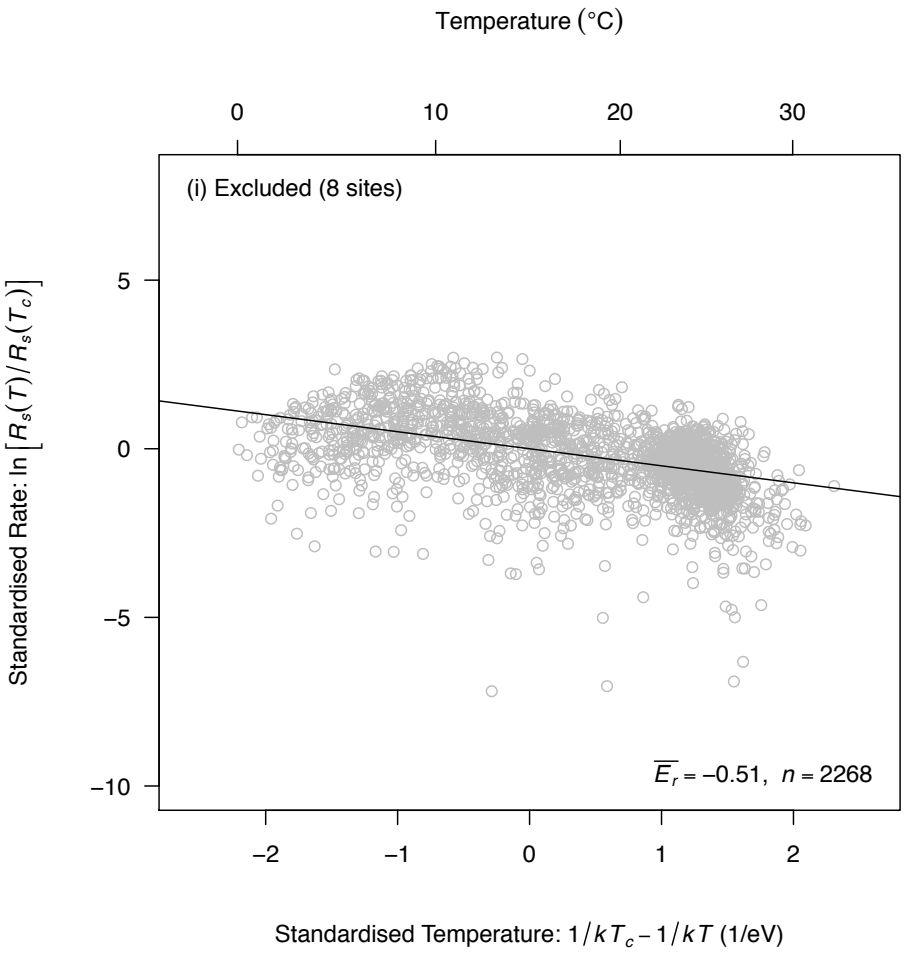

Figure S1.1. Relationship of standardised short-term respiration rate, $\ln\left[R_S(T)/R_S(T_C)\right]$, to standarised inverse temperature for the 8 terrestrial ecosystem sites that were excluded from our analysis. The site-specific estimates of respiration at fixed temperature, $R_S(T_C)$, and the average activation energies, $\overline{E_R}$, were determined using mixed-effects modelling (equation 1). The solid line corresponds to the fitted slope ($\overline{E_R}$). Analysis reveals that respiration declined with increasing temperature for these sites, which likely reflects the acute effects of increased water limitation during warmer months.

Table S1.1. Original data sources and attributes for the respiration measurements from FluxNet (forest, non-forest, and excluded ecosystems). The number *n* refers to the number of daily flux estimates for each site. Numbers are < 365 days because gap-filled estimates of flux were excluded from seasonal analyses, as were estimates obtained at air temperatures < 0°C.

Ecosystem Type	Site	Arithmetic Mean Annual Temperature (°C)	Temperature Range (°C)	*n*	Ref.
Forest					
	BE-Bra	11.2	24.7	292	12
	BE-Vie	7.3	29.5	232	13
	CA-Ca1	7.5	30.5	279	14
	CA-Ca2	6.8	25.6	276	14
	CA-Ca3	8.9	26.1	252	14
	CA-Oas	1.8	47.7	160	15
	CA-Ojp	0.7	56.1	163	16
	CA-Qfo	1.1	59.5	178	17
	CA-SJ2	-1.9	57.2	118	18
	CA-SJ3	0.6	55.6	150	18
	CA-TP4	8.0	42.6	196	19
	CA-WP1	0.5	49.4	217	20
	CN-Cha	3.4	47.2	159	21
	DE-Har	10.2	32.9	247	22
	DE-Meh	7.2	31.7	248	23
	DE-Tha	8.1	39.5	243	24
	DK-Sor	7.1	28.2	252	25
	FI-Hyy	2.5	40.3	174	26
	FI-Sod	0.0	52.1	129	27
	FR-Fon	10.6	30.3	269	28
	FR-Hes	9.5	36.7	277	28
	GF-Guy	24.9	4.7	333	29
	IT-Cpz	12.7	23.9	324	30
	IT-PT1	12.6	35.3	279	31
	IT-Ro1	15.1	24.0	266	32
	IT-Ro2	12.8	23.8	336	33
	IT-SRo	14.4	26.7	334	34
	SE-Nor	5.3	39.2	194	35
	UK-Ham	9.0	21.5	260	2
	US-Ho1	4.4	48.2	196	36
	US-Me3	6.8	31.2	246	37
	US-MMS	11.9	41.5	253	6
	US-MOz	12.8	42.3	273	38
	US-NR1	1.2	41.6	168	39
	US-PFa	5.4	50.9	174	40
	US-SP1	18.0	29.0	269	41

Table S1.1. Continued.

Non-forest Ecosystems					
	CA-Mer	5.5	46.2	189	42
	CH-Oe1	8.2	31.6	218	43
	CN-Do1	15.2	33.4	251	44
	CN-HaM	-3.4	36.1	136	45
	DE-Geb	8.5	26.6	260	46
	DE-Gri	6.3	38.2	189	47
	DK-Lva	7.7	24.9	228	47
	DK-Ris	6.2	24.3	241	2
	IT-MBo	3.1	35.5	190	48
	NL-Loo	9.0	33.2	282	49
	US-ARM	12.6	46.3	226	50
	US-IB2	11.0	45.7	222	51
	US-KS2	20.4	25.2	306	41
	US-SRM	16.6	31.1	333	52
Excluded					
	BR-Ban	25.7	11.8	257	2
	BR-Ji2	23.6	15.0	315	4
	BR-Sa1	23.9	5.0	262	53
	BR-Sa3	24.9	6.7	291	3
	PT-Mi2	12.4	28.8	303	5
	US-SO2	12.2	26.4	299	6
	US-Ton	14.0	27.0	264	8
	US-Var	12.4	26.4	277	54

Soils

Short- and long-term estimates of soil respiration were conducted using data compiled for a subset of studies listed in the soil respiration database (SRDB; http://code.google.com/p/srdb)[55]. For the analysis of short-term data, measurements of daily *in-situ* soil respiration and temperature were compiled here for the first time and comprised 4160 paired temperature-flux estimates taken at temperatures > 0°C for 46 sites across the globe (Appendix 1). As with the terrestrial ecosystem data, soil respiration measurements taken at below-freezing temperatures were excluded from the seasonal analysis.

The analysis of long-term data was conducted using annual respiration estimates obtained directly from SRDB (May 24, 2011 release date). Estimates

flagged as questionable in the databases were excluded (Quality _flags: Q10, Q11, Q12, Q13), as were estimates where the year of sampling (variable: Study_midyear) and/or the latitude-longitude coordinates of sampling were not reported. To evaluate the long-term temperature-dependence of respiration, we extracted 12 monthly estimates of average air temperature (January to December) for each SRDB flux estimate using SRDB-reported latitude-longitude coordinates and the year of the study. Monthly estimates of air temperature were obtained from the gridded (0.5x0.5° grid) database of Matsuura and Willmott (version 2.01, released June 2009), which was prepared using published methods[56], and is available online for the years 1900-2008 (http://climate.geog.udel.edu/~climate). Monthly estimates were interpolated to 365 daily estimates as described above. A relatively small number of SRDB flux estimates were dropped during the merger of SRDB with the climate database (~40) because sites were located on islands, or along the coast, and therefore fell outside the 0.5x0.5° grid. In order to avoid including multiple measurements from individual sites, only the first record for each study in the SRDB database was included in our analysis. A total 572 SRDB flux estimates were analysed here.

To ensure that using air temperature as a surrogate for soil temperature did not introduce biases into our long-term analysis of the SRDB data, it was necessary to compare estimates of kinetics obtained using air temperature versus soil temperature. To do this, we first digitised soil-temperature time series for a subset of the sites in the short-term analysis (n = 17) that had temperature measurements spanning ≥240 days, and that were also included in the long-term analysis (latitudinal range: -11.97°N to 53.12°N). We then separately interpolated the monthly air-temperature estimates and the digitised soil-temperature estimates, as described above, to obtain two one-year time series of 365 temperature values each. Finally, for each time series, we

calculated Boltzmann-averaged temperature kinetics as $\left\langle e^{E_P(1/kT_C - 1/kT)} \right\rangle_\tau = (1/\tau)\int_\tau e^{E_P(1/kT_C - 1/kT(t))} dt$, assuming $E_P = 0.32$, following Eq. 6 in the main text.

We found that the correlation between the air and soil estimates of Boltzmann averaged kinetics was highly significant ($r = 0.94$, $P < 10^{-8}$; Figure S1.2). More importantly, the slope of the relationship was not significantly different from 1 (95% CI: 0.93 - 1.17), and the intercept was not significantly different from 0 (95% CI: -0.20 to 0.07). This result implies that the air- and soil-temperature data exhibit an approximately 1:1 relationship with respect to Boltzmann-averaged temperature kinetics over a time period of 1 year, and therefore that both types of data should yield similar estimates for the temperature dependence of long-term respiration. This result justified our use of air temperature as a surrogate for soil temperature to assess whether the temperature dependence of long-term soil respiration (Figure 2c, Table 1; main text) had an effective activation energy of ~E_P, as predicted by Equation 6, and whether the temperature dependence of respiration at fixed temperature, $R(T_C)$, declined with increasing mean annual temperature (see section 10), as predicted by Eq. 7 (main text).

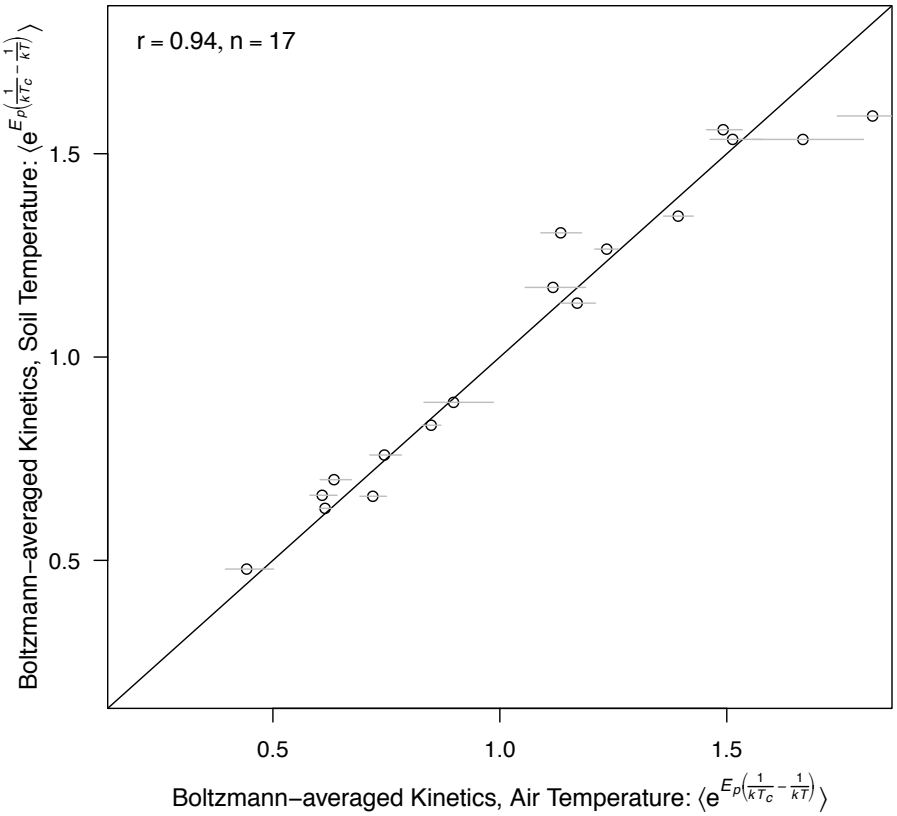

Figure S1.2. Relationship between estimates of Boltzmann-averaged temperature kinetics obtained using air and soil temperatures for 17 sites in the Soil Respiration Database (http://code.google.com/p/srdb)[55]. Air-temperature estimates were obtained from a published database[56]. Soil-temperature estimates were obtained by digitising data from figures in publications. Boltzmann-averaged temperature kinetics were calculated as $\left\langle e^{E_P(1/kT_C - 1/kT)} \right\rangle_\tau = (1/\tau)\int_\tau e^{E_P(1/kT_C - 1/kT(t))}dt$, where E_P = 0.32 eV (following Eq. 6 in the text). The relationship is approximately 1:1 (line in figure). Grey lines represent uncertainties in the estimates of Boltzmann-averaged temperature kinetics (95% CIs) that resulted from using spatially interpolated air temperatures. Confidence intervals were generated using the corresponding estimate of mean absolute error (MAE) for each monthly air temperature estimate, assuming (conservatively) that root

mean-squared error was double MAE, following results reported by Wilmott and Matsuura[57]. Confidence intervals were generated by: (1) adding a normally distributed random error with a standard deviation equal to twice the MAE, to each monthly temperature estimate; (2) linearly interpolating the simulated monthly temperature data for each site to obtain 365 daily estimates of temperature; (3) calculating Boltzmann-averaged temperature kinetics using the 365 estimates; (4) repeating this procedure 1000 times to estimate the 95% CIs. As shown graphically, simulations indicate that spatial interpolation introduced errors that were negligible relative to the range of variation in Boltzmann-averaged temperature kinetics.

Estuarine pelagic respiration

Measurements of respiration in the pelagic zones of estuaries and coastal areas are comprised of two large published datasets, one from Hopkinson & Smith[58] and the other from Caffrey *et al*.[59]. In total, this database includes 1018 measurements from 67 sites across the globe (see Appendix 1). The long-term analysis was conducted using only data from Caffrey *et al*. because data from all sites span at least 240 days of sampling, were collected using the same methodology, and span the entire coastal range of the USA, including the territory of Puerto Rico.

Estuarine benthic respiration

Measurements of sediment respiration in estuarine and coastal ecosystems across the globe were compiled as part of this study and comprise 443 measurements from 53 ecosystems, of which data from 17 sites are from the Danish National Aquatic Monitoring and Assessment Program (DNAMAP, https://oda.dk) (Appendix 1). The

long-term analysis was conducted using data for the subset of 45 sites with data spanning at least 240 days of sampling.

Lake pelagic respiration

Data on respiration rates in the pelagic zones of lakes were compiled as part of this study and comprise 3666 short-term measurements of temperature and flux from 95 sites. These data are given in Appendix 1, except for 9 sites from the GLEON network (Table S1.2). The compilation represents an extensive search of the published literature. Data were either extracted directly from tables in the manuscripts or digitised from the figures, except for when they were supplied directly by the authors. The long-term analysis was conducted using data for the subset of 17 sites with data spanning at least 240 days of sampling.

Table S1.2. Original data sources and attributes for the respiration measurements from GLEON (http://www.gleon.org/), which comprise 9 of the sites used in the Lake Pelagic analysis.

Ecosystem Type	Site	Arithmetic Mean Annual Temperature (°C)	Temperature Range (°C)	*n*	Ref.
Lake Pelagic					
	Annie	24.9	15.0	346	60
	Feeagh	12.4	15.3	243	60
	Kentucky	18.5	27.4	319	60
	Mirror	17.9	26.8	121	60
	Muggelsee	17.8	19.1	198	60
	Pontchartrain	21.1	28.9	218	60
	Rotoiti	25.7	10.4	68	60
	Rotorua	16.0	14.2	299	60
	YuanYang	14.6	11.4	217	60

Lake benthic respiration

The temperature dependence of sediment respiration in lakes was analysed using data compiled from the published literature. The majority of the data came from a compilation by Gudasz *et al.*[61], though a number of additional sites from across the globe were also included (see Appendix 1). This dataset comprised 428 short-term measurements of temperature and sediment respiration from 27 sites. Only *in-situ* measurements of respiration from natural ecosystems were included in our analysis; laboratory experimental studies were excluded. The long-term analysis was conducted using data for the subset of 17 sites with data spanning at least 240 days of sampling.

River respiration

Measurements of respiration in rivers and streams were compiled as part of this study and comprise 154 short-term measurements of temperature and flux from 24 sites (Appendix 1). The compilation represents an extensive, but not exhaustive, search of the published literature. Data were either extracted directly from tables in the manuscripts or digitised from the figures, except for when they were kindly supplied by the authors. The long-term analysis was conducted using data for the subset of 22 sites with data spanning at least 240 days of sampling.

Ocean microbial respiration

Data for microbial oceanic respiration concerns only the metabolism of the bacterial size fraction (<2μm) of the pelagic zones of marine ecosystems, which is typically >75% of total plankton metabolism[62] and is by far the most abundantly reported measurement of respiration in the marine literature. The data set analysed here is an

aggregation of the compilations of Robinson[62] and Rivkin and Legendre[63], with additional data from Alonso-Sáez *et al*.[64]. The combined dataset comprises 438 measurements of short-term microbial respiration from 26 sites (see Appendix 1). Annual rates of oceanic microbial respiration could not be estimated due to the paucity of data where respiration and temperature were measured over multiple seasons. Lack of temporal data at the site level also precluded determination of site-specific, short-term activation energies.

2. DERIVATION OF EQUATION (1)

The temperature dependence of ecosystem respiration at site *s*, $R_s(T)$, is characterized using the Boltzmann-Arrhenius relationship, $e^{-E_R/kT}$ (see Section 3 below for theoretical justification):

$$R_s(T) = R_o^s e^{-E_R/kT} \tag{S1}$$

Taking logarithms of both sides yields

$$\ln R_s(T) = E_R\left(1/kT_C - 1/kT\right) + \ln R_o^s - E_R/kT_C \tag{S2}$$

where $1/kT_C - 1/kT$ is standardised inverse absolute temperature for site *s*, and T_C (= 288 K = 15°C) is the temperature used to centre the temperature data, following equation (1) in the main text. The ecosystem-level normalisation for respiration, R_o^s, is expected to vary among sites, *s*, and may also vary within a site over time *t*, $R_o^s(t)$, and hence may covary with temperature variation through time at site *s*, $T_s(t)$ (K). Using standard formulae for the slope and intercept of a least-squares regression model, it can be shown that the best-fit linear function describing the relationship of $\ln R_o^s$ to $1/kT_C - 1/kT$ over the time interval is

$$\ln R_o^s = \frac{\mathrm{cov}[I_s, \ln R_o^s]_\tau}{\mathrm{var}[I_s]_\tau}\left[1/kT_C - 1/kT\right] + \left\langle \ln R_o^s \right\rangle_\tau - \frac{\mathrm{cov}[I_s, \ln R_o^s]_\tau}{\mathrm{var}[I_s]_\tau}\left\langle I_s \right\rangle_\tau \tag{S3}$$

where $\left\langle \ln R_o^s \right\rangle_\tau = (1/\tau)\int_\tau \ln R_o^s(t)dt$ and $\left\langle I_s \right\rangle_\tau = (1/\tau)\int_\tau I_s(t)dt$ are averages for $\ln R_o^s(t)$ and $I_s(t)$ over the time period τ, $I_s(t) \equiv 1/kT_C - 1/kT_s(t)$,

$\mathrm{var}[I_s]_\tau = (1/\tau)\int_\tau \left(I_s(t) - \left\langle I_s \right\rangle_\tau\right)^2 dt$ is the variance in $I_s(t)$, and

$\mathrm{cov}[I_s, \ln R_o^s]_\tau = (1/\tau)\int_\tau \left(I_s(t) - \left\langle I_s \right\rangle_\tau\right)\left(\ln R_o^s(t) - \left\langle \ln R_o^s \right\rangle_\tau\right)dt$ is the covariance between $I_s(t)$ and $\ln R_o^s(t)$. The apparent temperature-dependence of ecosystem respiration at

site *s* over this time interval, $\ln R_s(T)$, is obtained by combining equations (S2) and (S3) to yield

$$\ln R_s(T) = \left(E_R + \frac{\mathrm{cov}[I_s, \ln R_o^s]_\tau}{\mathrm{var}[I_s]_\tau}\right)\left(\frac{1}{kT_C} - \frac{1}{kT}\right) + \left\langle \ln R_o^s \right\rangle_\tau - E_R / kT_C - \left(\frac{\mathrm{cov}[I_s, \ln R_o^s]_\tau}{\mathrm{var}[I_s]_\tau}\right)\left\langle I_s \right\rangle_\tau \quad \text{(S4)}$$

Equation (S4) demonstrates that, if the ecosystem-level normalisation for respiration exhibits covariation with temperature over a time period τ, then the estimated apparent activation energy should equal $E_R + \mathrm{cov}[I_s, \ln R_o^s]_\tau / \mathrm{var}[I_s]_\tau$, rather than E_R, when data collected during that time period are combined for analysis.

In order to use this result to derive predictions for equation (1), it is important to note that this mixed-effects model is fitted so that site-specific deviations of the apparent activation energy, ε_E^s, have a mean of 0 when averaged across sites. Given this constraint, setting the slope in equation (1), $\overline{E_R} + \varepsilon_E^s$, equal to the slope in equation (S4), $E_R + \mathrm{cov}[I_s, \ln R_o^s]_\tau / \mathrm{var}[I_s]_\tau$, demonstrates that $\overline{E_R}$ is predicted to approximate the physiological temperature dependence of respiration (i.e. $E_R \approx 0.65$ eV) if the average across sites for $\mathrm{cov}[I_s, \ln R_o^s]_\tau / \mathrm{var}[I_s]_\tau$ is approximately equal to 0. Such a result would imply that constraints imposed by the activation energy of the respiratory complex override site-specific effects when analysing a collection of sites. It would also imply that the site-specific deviation in the apparent activation energy from E_R for a given site *s*, ε_E^s, is governed by covariance between $I_s(t)$ and $\ln R_o^s(t)$,

$$\varepsilon_E^s = \frac{\mathrm{cov}[\ln R_o^s, I_s]_\tau}{\mathrm{var}[I_s]_\tau} \quad \text{(S5)}$$

and that the site-specific deviation of the rate of ecosystem respiration at 15°C from $\overline{\ln R(T_C)}$, ε_R^s, is governed in part by this covariance,

$$\varepsilon_R^s = \left\langle \ln R_o^s \right\rangle_\tau - E_R / kT_C - \frac{\mathrm{cov}[\ln R_o^s, I_s]_\tau}{\mathrm{var}[I_s]_\tau} \left\langle I_s \right\rangle_\tau - \overline{\ln R(T_C)} \quad \text{(S6)}$$

and in part by community size structure through its effects on $\left\langle \ln R_o^s \right\rangle_\tau$.

3. DERIVATION OF EQUATIONS (2) - (5)

Respiration is the primary catabolic pathway that fuels the survival, growth and reproduction of organisms. Individual body mass, m_i (g C), and absolute temperature, T (in K), are the primary determinants of individual respiration, r_i (g C d^{-1}). The combined effects of these variables are predicted by metabolic theory[66] using the equation

$$r_i = r_o m_i^{\alpha} e^{-E_R/kT} \quad \text{(S7)}$$

where r_o is an individual-level normalisation for respiration ($g^{1-\alpha}$ C d^{-1}). This size dependence reflects changes in the density of respiratory complexes per unit mass[65] and is characterised by an exponent α that is typically near 3/4 for metazoans[67], but may be considerably steeper for unicellular prokaryotes and eukaryotes[68]. The temperature dependence, characterised by the Boltzmann factor, $e^{-E_R/kT}$, reflects the exponential effects of temperature, T (K), on the kinetics of biochemical reactions in the respiratory complex, where k is the Boltzmann constant (8.62×10^{-5} eV K^{-1}) and E_R is an activation energy (1 eV = 96.49 kJ mol^{-1}). The Boltzmann factor is consistent with principles of physical chemistry[69] and with the observation that the proportional increase in rate per 10°C increase in temperature (i.e. Q_{10}) declines as temperature increases[70,71]. Comparative studies indicate that this temperature dependence, characterised by E_R, is essentially the same at the subcellular and individual levels[72], and that E_R takes a narrow range of values for diverse taxa including autotrophs and unicellular and multicellular heterotrophs (~0.6 – 0.7 eV)[66]. See, for example, the study of Tjoelker *et al.*[73], which demonstrates that Q_{10} declines with increasing temperature for plant respiration, as predicted by the Boltzmann

relationship, and that Q_{10} at 15°C for plant respiration is ~2.5, which corresponds to an activation energy of ~0.65 eV.

Due to mass and energy balance, the rate of respiration per unit area, $R_P(T)$ (g C m^{-2} d^{-1}), by a biomass pool, *P*, is equal to the sum of the respiratory fluxes, r_i^P, characterised by equation (S1), for all *J* individuals in an area of size *A*,

$$R_P(T) = (1/A)\sum_{i=1}^{J} r_i^P = (J/A) r_o^P \left\langle m_P^\alpha \right\rangle e^{-E_R/kT} = r_o^P M_P \left\langle m_P^{\alpha-1} \right\rangle e^{-E_R/kT} \quad \text{(S8)}$$

where r_o^P is the individual-level normalisation for respiration, which can differ between autotrophs and heterotrophs[66]. In this expression, M_P is total biomass per unit area in the pool $\left(= (1/A)\sum_{i=1}^{J} m_i = (J/A)\langle m_P \rangle\right)$, $\langle m_P \rangle$ is the average body mass of individuals $\left(= (1/J)\sum_{i=1}^{J} m_i\right)$, $\left\langle m_P^\alpha \right\rangle$ is the average of m_i^α for individuals $\left(= (1/J)\sum_{i=1}^{J} m_i^\alpha\right)$, and $\left\langle m_P^{\alpha-1} \right\rangle$ is an average for $m_i^{\alpha-1}$ weighted by biomass rather than individual abundance[65] $\left(= (1/(AM_P))\sum_{i=1}^{J} m_i^\alpha = \left\langle m_P^\alpha \right\rangle / \langle m_P \rangle\right)$. In equation (S8), $M_P \left\langle m_P^{\alpha-1} \right\rangle$ is mass-corrected biomass. Mass correction, by $\left\langle m_P^{\alpha-1} \right\rangle$, is necessary to account for changes in the density of metabolic units per unit mass– e.g. mitochondria or chloroplasts – with body mass[74]. Ecosystem respiration, $R(T)$, is calculated by separately summing the individual respiration rates for autotrophs, *A*, and heterotrophs, *H*,

$$R(T) = R_A(T) + R_H(T) = R_o e^{-E_R/kT} \quad \text{(S9a)}$$

following equation (S8), where

$$R_o = r_o^A M_A \left\langle m_A^{\alpha-1} \right\rangle + r_o^H M_H \left\langle m_H^{\alpha-1} \right\rangle \quad \text{(S9b)}$$

is the ecosystem-level respiratory normalisation. Equations (S8) and (S9) yield equations (2)-(5) in the text. Equation S9 entails the simplifying assumption that autotrophs and heterotrophs experience similar environmental conditions with respect to Boltzmann temperature kinetics. Figure S1.2 (in section 1 above) indicates that this assumption is reasonable given the broad range of temperature regimes encompassed by sites in our analysis.

4. DERIVATION OF EQUATIONS (6) - (7)

For ecosystems where respiration is limited by, and therefore directly coupled to, gross primary production, annual respiration is governed by the temperature dependence of photosynthesis. At the level of the autotroph individual, the combined effects of size and temperature on the gross rate of individual-level photosynthesis at time t, p_i, are characterised by

$$p_i \approx p_o m_i^{\alpha} e^{-E_P / kT} \tag{S10}$$

where p_o is a normalisation constant ($g^{1-\alpha}$ C h^{-1}), independent of body mass and temperature[65,75,76]. The size dependence for p_i reflects theory and data indicating that the density of chloroplasts declines with increasing plant size[77]. The temperature dependence is approximated using an "effective" activation energy, $E_P \approx 0.32$ eV, to facilitate direct comparisons with the exponential temperature dependence of respiration. We refer to E_P as an effective activation energy because photosynthesis is neither predicted nor observed to exhibit exponential temperature dependence[78]. Nevertheless, this two-parameter expression is an excellent approximation of the well-established 8-parameter model of Farquhar *et al.*[78] at temperatures < 30°C (Ref. 65), and both functions yield a Q_{10} of ~1.6 at 15°C based on the temperature dependence of Rubisco carboxylation in chloroplasts[65]. While this prediction was derived *a priori* based on the biochemical kinetics of Rubisco carboxylation in land plants[65], empirical data indicate that this temperature dependence also applies to algae[75,76]. We therefore assume that equation (S10) applies to aquatic plants as well.

Short-term imbalances between photosynthate production and consumption by respiration can and do occur within plants. However, over the long term, individual-level autotroph respiration, r_i^A,

$$r_i^A = r_o^A m_i^\alpha e^{-E_R/kT} \quad \text{(S11)}$$

is ultimately limited by the production of reduced carbon substrates via individual-level photosynthesis, p_i (equation S10), with its weaker temperature dependence[80].

Consequently, the individual-level normalisation for autotroph respiration, r_o^A (equation S9b), must decline with long-term (e.g. weeks to months) temperature increases. We can derive zeroth-order predictions for this well-established phenomenon of "type II respiratory acclimation"[71] by noting that the fraction of photosynthate that a plant allocates to respiration, $1-\varepsilon$, is largely independent of temperature over long time intervals[76], such as $\tau = 1$ yr. Thus, the long-term temperature dependence of r_o^A can be approximated by first integrating individual-level expressions for photosynthate production allocated to autotroph respiration, $(1-\varepsilon)p_i$ (equation S10),

$$\tau(1-\varepsilon)\langle p_i\rangle_\tau = (1-\varepsilon)\int_\tau p_o m_i^\alpha e^{-E_P/kT(t)}dt = \tau(1-\varepsilon)p_o m_i^\alpha \left\langle e^{-E_P/kT}\right\rangle_\tau \quad \text{(S12)}$$

and photosynthate consumption by autotroph respiration, r_i^A (equation S11),

$$\tau\langle r_i^A\rangle_\tau = \int_\tau r_o^A m_i^\alpha e^{-E_R/kT(t)}dt = \tau r_o^A m_i^\alpha \left\langle e^{-E_R/kT}\right\rangle_\tau \quad \text{(S13)}$$

with respect to temperature variation through time, $T(t)$, over the time interval τ, and then setting $\tau(1-\varepsilon)\langle p_i\rangle_\tau$ equal to $\tau\langle r_i^A\rangle_\tau$ to yield[65]

$$r_o^A = (1-\varepsilon)p_o \left\langle e^{-E_P/kT}\right\rangle_\tau \Big/ \left\langle e^{-E_R/kT}\right\rangle_\tau \quad \text{(S14)}$$

where $\left\langle e^{-E_P/kT}\right\rangle_\tau = (1/\tau)\int_\tau e^{-E_P/kT(t)}dt$. Empirical data from terrestrial plants indicate that r_o^A is insensitive to diurnal temperature fluctuations, but declines in response to temperature increases that are weeks to months in duration[80,81]. Thus, equation (S14) is a reasonable approximation over longer time intervals, such $\tau = 1$ yr.

The rate of gross primary production is obtained by summing the individual-level photosynthetic rates, p_i, for all the autotrophs in the ecosystem, following equations (S8) and (S10),

$$P(T) = (1/A)\sum_{i=1}^{J} p_i = p_o M_{Tot}^{A} \left\langle m_A^{\alpha-1} \right\rangle e^{-E_P/kT} \tag{S15}$$

Annual gross primary production, $\tau\langle P(T)\rangle_\tau$, is obtained by integrating seasonal variation in temperature, $T(t)$, in the expression above over the time interval τ, which yields equation (6) in the main text. Annual respiratory fluxes for autotrophs, $\tau\langle R_A(T)\rangle_\tau$, are obtained by performing a similar integration using equations (S8), (S11), and (S14) to yield

$$\begin{aligned} \tau\langle R_A(T)\rangle_\tau &= \int_\tau R_A(T(t))dt = \tau r_o^A M_A \left\langle m_A^{\alpha-1} \right\rangle \left\langle e^{-E_R/kT} \right\rangle_\tau = \\ &= \tau(1-\varepsilon)\langle P(T)\rangle_\tau = \tau(1-\varepsilon) p_o M_A \left\langle m_A^{\alpha-1} \right\rangle \left\langle e^{-E_P/kT} \right\rangle_\tau \end{aligned} \tag{S16}$$

In the expression above, differences in the temperature dependence of autotroph respiration over the short term (E_R) and long term (E_P) are reconciled through declines in the individual-level normalisation for autotroph respiration, r_o^A, with long-term (weeks to months) temperature increases $\left(\propto \left\langle e^{-E_P/kT} \right\rangle_\tau \Big/ \left\langle e^{-E_R/kT} \right\rangle_\tau\right)$, following equation (S14). By contrast, for heterotrophs, the individual-level normalisation for respiration, r_o^H, is approximately independent of temperature because energy acquisition and consumption by a heterotroph is fuelled by its own respiration[65]. Consequently, differences in the temperature dependence of respiration and photosynthesis are instead reconciled through declines in heterotroph abundance and biomass with long-term temperature increases,

$$M_H \left\langle m_H^{\alpha-1} \right\rangle = (\theta - 1 + \varepsilon)(p_o / r_o^H) M_A \left\langle m_A^{\alpha-1} \right\rangle \left\langle e^{-E_P/kT} \right\rangle_\tau \Big/ \left\langle e^{-E_R/kT} \right\rangle_\tau \tag{S17}$$

where θ is the fraction of gross primary production respired by autotrophs and heterotrophs, which is assumed to be temperature-independent. These declines occur because individual-level metabolic demands of heterotrophs increase more rapidly with temperature than ecosystem net primary production, $\tau\varepsilon\langle P(T)\rangle_\tau$. In this way, annual heterotroph respiration, $\tau\langle R_H(T)\rangle_\tau$, can increase linearly with annual net primary production despite predicted fundamental differences in the temperature dependencies of photosynthesis and respiration:

$$\begin{aligned}\tau\langle R_H(T)\rangle_\tau &= \int_\tau R_H(T(t))dt = \tau r_o^H M_H \left\langle m_H^{\alpha-1}\right\rangle\left\langle e^{-E_R/kT}\right\rangle_\tau = \\ &= \tau(\theta-1+\varepsilon)\langle P(T)\rangle_\tau = \tau(\theta-1+\varepsilon)p_o M_A\left\langle m_A^{\alpha-1}\right\rangle\left\langle e^{-E_P/kT}\right\rangle_\tau\end{aligned} \quad \text{(S18)}$$

In equation (6), $\tau\langle R(T)\rangle_\tau$ is obtained by summing $\tau\langle R_A(T)\rangle_\tau$ and $\tau\langle R_H(T)\rangle_\tau$ in equations (S16) and (S18). In Equation (7), $R(T_C)$ is obtained from equation (S9b) by replacing r_o^A with $(1-\varepsilon)p_o\left\langle e^{-E_P/kT}\right\rangle_\tau\Big/\left\langle e^{-E_R/kT}\right\rangle_\tau$, following equation (S14), and by replacing $M_H\left\langle m_H^{\alpha-1}\right\rangle$ with $(\theta-1+\varepsilon)(p_o/r_o^H)M_A\left\langle m_A^{\alpha-1}\right\rangle\left\langle e^{-E_P/kT}\right\rangle_\tau\Big/\left\langle e^{-E_R/kT}\right\rangle_\tau$, following equation (S17).

5. SHORT-TERM STATISTICAL ANALYSES

Mixed-effects modelling is used to quantify relationships between a response variable and covariates, which can have a nested covariance structure and may be unbalanced[82]. The parameters in equation (1) were estimated by fitting mixed-effects models to the short-term respiration data using the function *lmer* in the lme4 package of R statistical software[83]. These analyses allowed us to determine the average temperature dependence of ecosystem respiration, $\overline{E_R}$, for each of the nine ecosystem types, as well as an overall global estimate for all ecosystem types combined. For these analyses, we adopted a top-down approach, starting with the most complex model, to determine the significance of the fixed and random effects in a two-stage analysis. In stage one, we determined the correct random-effects structure of the data. The most complex random-effects structure included random variation in both E_R and $\ln R(T_c)$ attributable to sites. The simplest random-effects structure included only variation in $\ln R(T_c)$ attributable to sites. By comparing models of progressively reduced complexity using AIC tests, the final model was determined as the one having the lowest AIC score[84,85]. Analysis revealed that the random-effects structure that best described the combined dataset of nine ecosystem types included random variation in $\overline{E_R}$ and $\ln R(T_C)$ attributable to sites (see Model R2 of Table S5 below).

In the second stage of the analysis, we applied the random-effects structure determined in stage one to a range of fixed-effects structures to assess the significance of differences in $\overline{E_R}$ and $\overline{\ln R(T_C)}$ between ecosystem types. Models were compared using the likelihood ratio test. The analysis revealed that $\overline{\ln R(T_C)}$, but not $\overline{E_R}$, varied significantly between ecosystem types. Thus, the best model was Model F1 (Table S3), which yielded an overall activation energy for ecosystem respiration (0.62 eV,

95% CI: 0.60 - 0.66 eV; Table 1, main text) that is indistinguishable from the predicted value of ~0.65 eV.

A series of independent analyses was also carried out to determine the seasonal temperature dependence of respiration for each ecosystem type separately (results summarised in Table 1, main text). Again, the nested structure and unbalanced nature of the data necessitated the use of mixed-effects models. In this analysis, both E_R and $\ln R(T_C)$ were allowed to vary randomly between ecosystems in the most complex model, and the significance of each term was assessed, as above, by comparing models with either random variation in E_R or $\ln R(T_C)$ only with the most complex model using likelihood ratio tests tests. For each ecosystem type, E_R and $\ln R(T_C)$ varied significantly between sites, as revealed by the significance of the random effects terms in the likelihood ratio tests (Table 1 main text). No attempt was made to determine site-specific estimates of E_R for the oceanic microbial data due to limited seasonal temperature variation at individual sites.

Table S5. Mixed-effects analysis of data from all ecosystem types combined. Models R1 and R2 were fit using restricted maximum likelihood (REML) and AIC tests were used to compare models. Models F1 and F2 were fit using maximum likelihood (ML) and likelihood ratio tests were used to determine the significance of model parameters by comparing restricted models to more complex models. Parameters in the final model were then assessed by refitting the model using REML. In Stage 1, results revealed that Model R2 had the random-effects structure that best described the data. Model R2 included random variation in E_R and $\ln R(T_C)$ attributable to sites. In Stage 2, results revealed that Model F1 had the fixed-effect structure that best described the data, given the random-effects structure (model R2). Model F1 includes ecosystem-type differences with respect to $\overline{\ln R(T_C)}$, as expected, but not $\overline{E_R}$. The *P*-values of the likelihood ratio tests are read from the table as follows: in Stage 2, the more complex model F2 is not a significantly better fit to the data than model F1.

Model	**DF**	**AIC**	**logLik**	χ^2	***P***
Random-effects structure					
R1. $\ln R(T_C)$ * site	20	54298			
R2. E_R*site + $\ln R(T_C)$ * site	21	52286			
***Fixed-effects structure* (*given random structure*=R2)**					
F1. E_R + type | random=R2	13	52278	-26126		
F2. E_R * type | random=R2	21	52286	-26122	7.36	0.50

6. LONG-TERM STATISTICAL ANALYSES

Equation (6) predicts that annual respiration increases proportionally with Boltzmann-averaged temperature kinetics for photosynthesis, $\left\langle e^{E_P(1/kT_C - 1/kT)} \right\rangle_\tau = (1/\tau)\int e^{E_P(1/kT_C - 1/kT(t))} dt$, over the time interval τ = 1 year. In general, for any given activation energy E, $\left\langle e^{-E/kT} \right\rangle_\tau \neq e^{-E/k\langle T \rangle_\tau}$ where $\langle T \rangle_\tau$ is mean annual temperature. Moreover, the approximation $\left\langle e^{-E/kT} \right\rangle_\tau \approx e^{-E/k\langle T \rangle_\tau}$ becomes less accurate as temperature variation increases[86]. Thus, to obtain the most accurate estimate for the activation energy, E, and ecosystem-level normalization, F_o, for long-term flux, it is preferable to directly analyse the integrated Boltzmann factor, particularly if the analysis includes sites that exhibit substantial variation in temperature. To achieve this goal, we applied the method of maximum likelihood as follows:

1. Select values of E and F_o for consideration.
2. Given E, calculate Boltzmann-averaged temperature kinetics, B_s, for each site s based on its temperature variation through time, $T_s(t)$, as $B_s = (1/\tau)\int_\tau e^{E(1/kT_C - 1/kT_s(t))} dt$.
3. Given F_o and B_s, calculate the predicted annual flux as $P_s = \tau F_o B_s$ for each site s.
4. Given the predicted values, P_s, and observed annual fluxes, O_s, for all n sites, calculate the log-likelihood, L, as $L = \sum_{s=1}^{n} f(\ln O_s - \ln P_s)$, where $f(\ln O_s - \ln P_s)$ is the log of the probability density for a deviation of magnitude $\ln O_s - \ln P_s$ from a normal distribution of mean 0.

5. Repeat steps (1) – (4) using different values of E and F_o until the parameter estimates that maximize L have been found.

For each of the 8 ecosystem types depicted in Figure 2, we estimated E and F_o using the *mle*2 function in the bbmle package for R statistical software[83].

7. ACCOUNTING FOR GROWING SEASON LENGTH

As noted by Enquist[87], when assessing the effects of temperature on ecosystem metabolism along broad-scale geographic gradients, it is important to control for growing season length and daylight hours during the growing season, both of which are often confounded with mean annual temperature. This issue is particularly important when analysing data for terrestrial systems because high-latitude terrestrial sites not only have lower mean annual temperatures, but also shorter plant growing seasons when temperatures exceed 0°C, as compared to low-latitude sites. This issue is readily addressed using our maximum likelihood approach (described above). To do so, we replace the Boltzmann-averaged kinetics, B_s, with the following expression, $B_s^{'}$, in step (2),

$$B_s^{'} = (1/\tau)\int_{\tau} D(t)G(t)e^{E(1/kT_C - 1/kT_s(t))}dt \quad \text{(S19)}$$

and we replace predicted flux, P_s, with the following expression, $P_s^{'}$, in step (3):

$$P_s^{'} = \tau F_o B_s^{'} \quad \text{(S20)}$$

In these expressions, $D(t)$, is an indicator function that takes a value of 1 during daylight hours and 0 at night, and $G(t)$ an indicator function that takes a value of 1 during the growing season and 0 otherwise.

To verify our finding that the temperature dependence of annual ecosystem respiration in terrestrial ecosystems closely matched the predicted temperature dependence of photosynthesis for soils and forests, we carried out an additional long-term analysis with the forest and soil data using the expressions for $B_s^{'}$ for $P_s^{'}$ above. To do this, we obtained site-specific expressions for $D(t)$ by defining the growing season as including days when average temperatures were >0°C, and site-specific expressions for $G(t)$ by estimating the number of daylight hours on each day of the

year from the geographic coordinates using a published function[88]. The results of this analysis are given in Table S7, and reveal that growing season correction does not substantially affect the temperature dependence, consistent with the recent findings of Chen *et al*.[89] for plant respiration.

Table S7. Results of growing season corrected long-term maximum likelihood analysis of the temperature dependence of terrestrial ecosystem respiration.

Ecosystem Type	***E* (95% CI)**	r^2	***P***	***n* sites**
Forest	0.28 (0.06 – 0.50)	0.50	<0.05	38
Soil	0.26 (0.18 – 0.33)	0.19	<0.005	572

8. CORRELATION BETWEEN THE SEASONAL ACTIVATION ENERGY AND AVERAGE TEMPERATURE

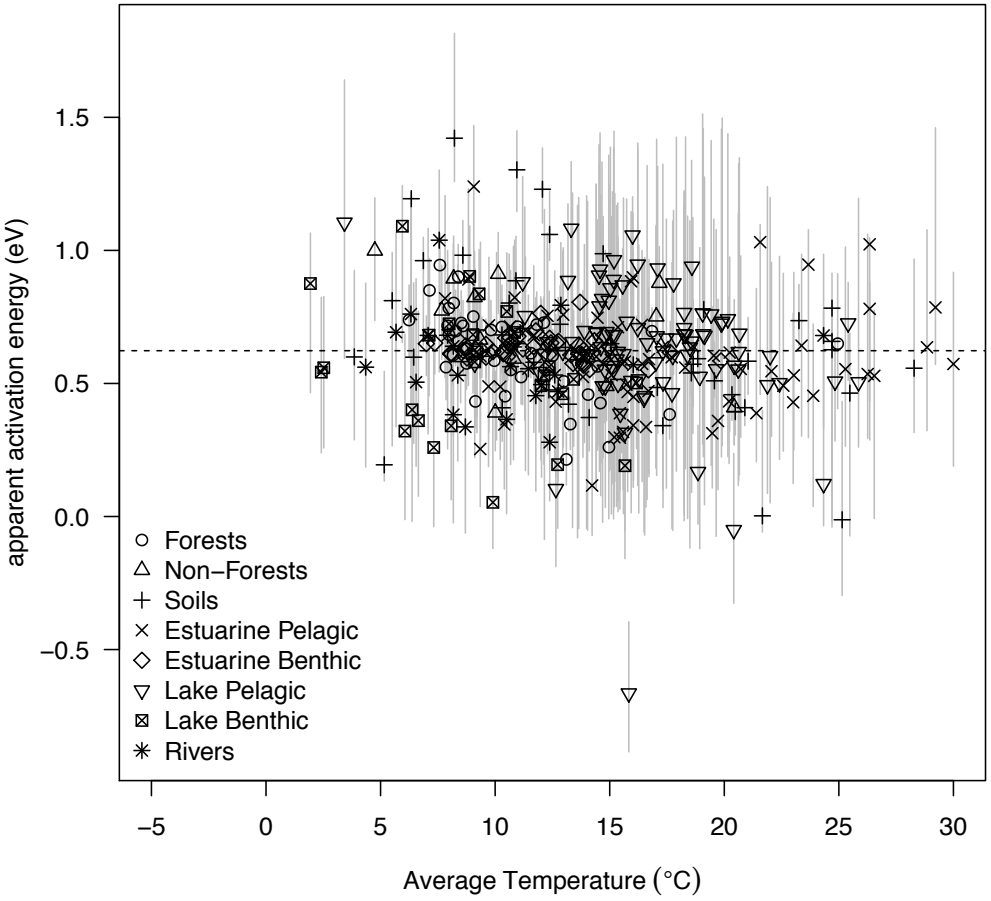

Relationship of the estimated apparent activation energy of short-term ecosystem respiration to average site temperature (note temperatures <0°C were excluded from the short-term analysis; see section 1 for details) for ecosystems included in our mixed-effects modelling analysis (n = 347; estimates for oceanic sites could not be calculated due to insufficient seasonal data). Grey lines correspond to 95% confidence intervals. The relationship between the two variables is significant ($P < 0.05$), but weak ($r^2 = 0.02$). The dashed line is the average activation energy for all sites, as estimated by mixed-effects analysis (0.62 eV, Table 1).

9. VARIABILITY IN THE SEASONAL ACTIVATION ENERGY FOR EACH ECOSYSTEM TYPE

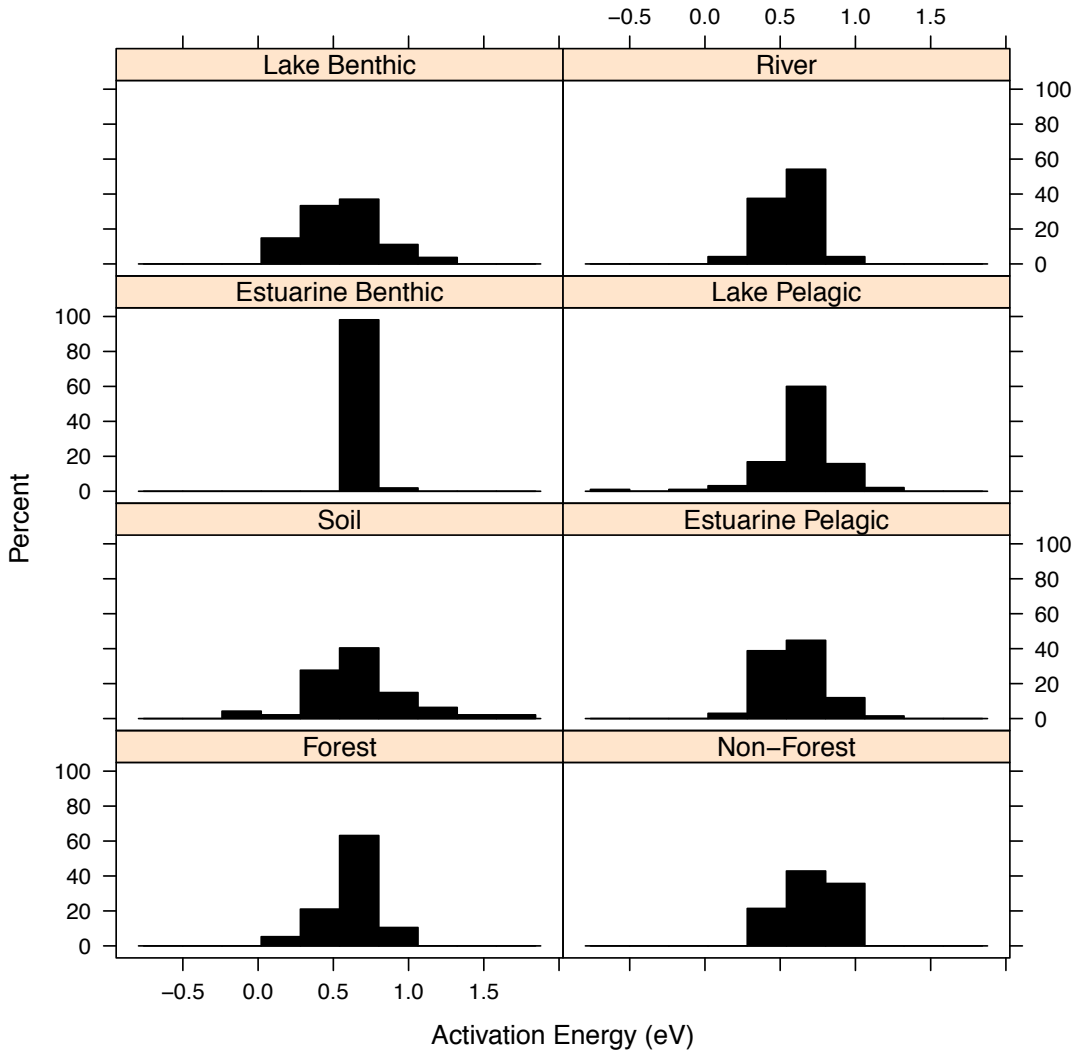

Histograms of the seasonal activation energies, E_R, of ecosystem respiration for each ecosystem type. Data reveal variability in the apparent activation energy among sites within each ecosystem type, which is predicted by equations (S4) - (S6) when the site-level normalisation constant exhibits seasonal covariation with temperature (see Section 2).

10. CORRELATION BETWEEN THE AVERAGE RESPIRATION RATES AT 15°C AND AVERAGE SITE TEMPERATURE

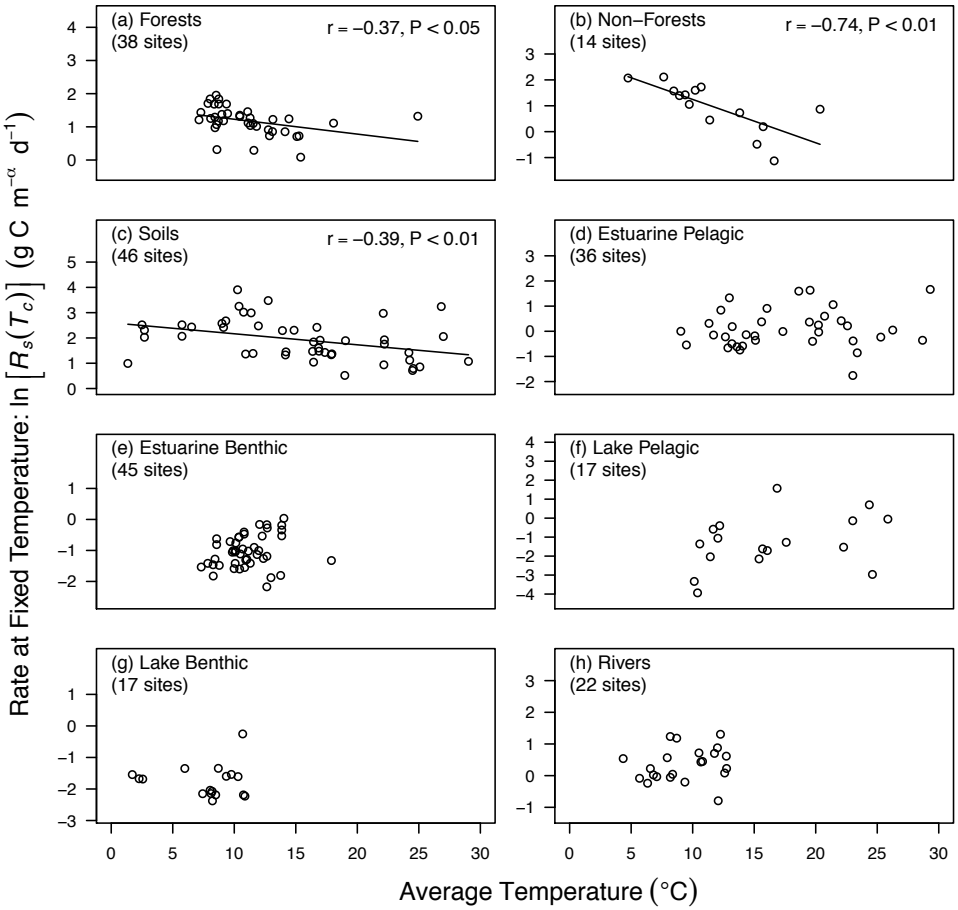

Relationship between average daily respiration rate at 15°C and average site temperature. Average temperature was calculated as the arithmetic mean, using only temperature data >0°C, for consistency with methods used to estimate $\ln R(T_C)$ in the short-term analyses (see section 1). Only sites that were also included in the long-term analyses are analysed here. Correlations between the two variables were significant and negative for all of the terrestrial ecosystems ($P < 0.05$), as predicted by equation (6) in the main text, but were not significant for any of the aquatic ecosystems ($P > 0.05$). These findings serve to reconcile striking similarities in the short-term temperature dependence of ecosystem respiration for terrestrial and aquatic

ecosystems (Fig. 1, main text) with pronounced differences in long-term rates (Fig. 2, main text).

REFERENCES

1. Bond-Lamberty, B. & Thomson, A. A global database of soil respiration data. *Biogeosciences* **7**, 1915–1926 (2010).
2. Mahecha, M.D. et al. Global Convergence in the Temperature Sensitivity of Respiration at Ecosystem Level. *Science* **329**, 838–840 (2010).
3. Goulden, M. et al. Diel and seasonal patterns of tropical forest CO2 exchange. *Ecol Appl* **14**, S42–S54 (2004).
4. Kruijt, B. et al. The robustness of eddy correlation fluxes for Amazon rain forest conditions. *Ecol Appl* **14**, S101–S113 (2004).
5. Pereira, J.S. et al. Net ecosystem carbon exchange in three contrasting Mediterranean ecosystems - the effect of drought. *Biogeosciences* **4**, 791–802 (2007).
6. Lipson, D., Wilson, R. & Oechel, W. Effects of elevated atmospheric CO2 on soil microbial biomass, activity, and diversity in a chaparral ecosystem. *Applied and Environmental Microbiology* **71**, 8573–8580 (2005).
7. Xu, L. & Baldocchi, D. Seasonal variation in carbon dioxide exchange over a Mediterranean annual grassland in California. *Agricultural and Forest Meteorology* **123**, 79–96 (2004).
8. Ma, S., Baldocchi, D.D., Xu, L. & Hehn, T. Inter-annual variability in carbon dioxide exchange of an oak/grass savanna and open grassland in California. *Agricultural and Forest Meteorology* **147**, 157–171 (2007).
9. Papale, D. et al. Towards a standardized processing of Net Ecosystem

Exchange measured with eddy covariance technique: algorithms and uncertainty estimation. *Biogeosciences* **3**, 571–583 (2006).

10. Graf, A., Weihermuller, L., Huisman, J.A., Herbst, M. & Vereecken, H. Comment on "Global Convergence in the Temperature Sensitivity of Respiration at Ecosystem Level." *Science* **331**, 1265–1265 (2011).
11. Monson, R. et al. Winter forest soil respiration controlled by climate and microbial community composition. *Nature* **439**, 711–714 (2006).
12. Carrara, A. Seasonal changes in photosynthesis, respiration and NEE of a mixed temperate forest. *Agricultural and Forest Meteorology* **126**, 15–31 (2004).
13. Aubinet, M. et al. Long term carbon dioxide exchange above a mixed forest in the Belgian Ardennes. *Agricultural and Forest Meteorology* **108**, 293–315 (2001).
14. Humphreys, E.R. et al. Carbon dioxide fluxes in coastal Douglas-fir stands at different stages of development after clearcut harvesting. *Agricultural and Forest Meteorology* **140**, 6–22 (2006).
15. Black, T. et al. Increased carbon sequestration by a boreal deciduous forest in years with a warm spring. *Geophys. Res. Lett.* **27**, 1271–1274 (2000).
16. Howard, E., Gower, S., Foley, J. & Kucharik, C. Effects of logging on carbon dynamics of a jack pine forest in Saskatchewan, Canada. *Global Change Biology* **10**, 1267–1284 (2004).
17. Bergeron, O. et al. Comparison of carbon dioxide fluxes over three boreal black spruce forests in Canada. *Global Change Biology* **13**, 89–107 (2007).
18. Zha, T. et al. Carbon sequestration in boreal jack pine stands following harvesting. *Global Change Biology* **15**, 1475–1487 (2009).

19. Arain, A. & Restrepo-Coupe, N. Net ecosystem production in a temperate pine plantation in southeastern Canada. *Agricultural and Forest Meteorology* **128**, 223–241 (2005).

20. Syed, K.H., Flanagan, L.B., Carlson, P.J., Glenn, A.J. & Van Gaalen, K.E. Environmental control of net ecosystem CO2 exchange in a treed, moderately rich fen in northern Alberta. *Agricultural and Forest Meteorology* **140**, 97–114 (2006).

21. Guan, D.-X. et al. CO2 fluxes over an old, temperate mixed forest in northeastern China. *Agricultural and Forest Meteorology* **137**, 138–149 (2006).

22. Schindler, D., Tuerk, M. & Mayer, H. CO2 fluxes of a Scots pine forest growing in the warm and dry southern upper Rhine plain, SW Germany. *Eur J Forest Res* **125**, 201–212 (2006).

23. Don, A., Rebmann, C., Kolle, O., Scherer-Lorenzen, M. & Schulze, E.-D. Impact of afforestation-associated management changes on the carbon balance of grassland. *Global Change Biology* **15**, 1990–2002 (2009).

24. Gruenwald, T. & Bernhofer, C. A decade of carbon, water and energy flux measurements of an old spruce forest at the Anchor Station Tharandt. *Tellus B* **59**, 387–396 (2007).

25. Pilegaard, K. et al. Field measurements of atmosphere-biosphere interactions in a Danish beech forest. *Boreal Environ Res* **8**, 315–333 (2003).

26. Tanja, S. et al. Air temperature triggers the recovery of evergreen boreal forest photosynthesis in spring. *Global Change Biology* **9**, 1410–1426 (2003).

27. Suni, T. et al. Long-term measurements of surface fluxes above a Scots pine forest in Hyytiala, southern Finland, 1996-2001. *Boreal Environ Res* **8**, 287–301 (2003).

28. Granier, A. et al. The carbon balance of a young Beech forest. *Functional Ecology* **14**, 312–325 (2000).

29. Bonal, D. et al. Impact of severe dry season on net ecosystem exchange in the Neotropical rainforest of French Guiana. *Global Change Biology* **14**, 1917–1933 (2008).

30. Garbulsky, M.F., Penuelas, J., Papale, D. & Filella, I. Remote estimation of carbon dioxide uptake by a Mediterranean forest. *Global Change Biology* **14**, 2860–2867 (2008).

31. Migliavacca, M. et al. Seasonal and interannual patterns of carbon and water fluxes of a poplar plantation under peculiar eco-climatic conditions. *Agricultural and Forest Meteorology* **149**, 1460–1476 (2009).

32. Rey, A. et al. Annual variation in soil respiration and its components in a coppice oak forest in Central Italy. *Global Change Biology* **8**, 851–866 (2002).

33. Tedeschi, V. et al. Soil respiration in a Mediterranean oak forest at different developmental stages after coppicing. *Global Change Biology* **12**, 110–121 (2006).

34. Chiesi, M. et al. Modelling carbon budget of Mediterranean forests using ground and remote sensing measurements. *Agricultural and Forest Meteorology* **135**, 22–34 (2005).

35. Lagergren, F. et al. Biophysical controls on CO2 fluxes of three Northern forests based on long-term eddy covariance data. *Tellus B* **60**, 143–152 (2008).

36. Hollinger, D. et al. Spatial and temporal variability in forest-atmosphere CO2 exchange. *Global Change Biology* **10**, 1689–1706 (2004).

37. Irvine, J. & Law, B. Contrasting soil respiration in young and old-growth ponderosa pine forests. *Global Change Biology* **8**, 1183–1194 (2002).

38. Gu, L. et al. Direct and indirect effects of atmospheric conditions and soil moisture on surface energy partitioning revealed by a prolonged drought at a temperate forest site. *J Geophys Res-Atmos* **111**, – (2006).

39. Monson, R. et al. Carbon sequestration in a high-elevation, subalpine forest. *Global Change Biology* **8**, 459–478 (2002).

40. Davis, K. et al. The annual cycles of CO2 and H2O exchange over a northern mixed forest as observed from a very tall tower. *Global Change Biology* **9**, 1278–1293 (2003).

41. Powell, T.L. et al. Carbon exchange of a mature, naturally regenerated pine forest in north Florida. *Global Change Biology* **14**, 2523–2538 (2008).

42. Lafleur, P., Roulet, N., Bubier, J., Frolking, S. & Moore, T. Interannual variability in the peatland-atmosphere carbon dioxide exchange at an ombrotrophic bog. *Global Biogeochem. Cycles* **17**, (2003).

43. Ammann, C., Flechard, C.R., Leifeld, J., Neftel, A. & Fuhrer, J. The carbon budget of newly established temperate grassland depends on management intensity. *Agriculture Ecosystems & Environment* **121**, 5–20 (2007).

44. Yan, Y. et al. Closing the carbon budget of estuarine wetlands with tower-based measurements and MODIS time series. *Global Change Biology* **14**, 1690–1702 (2008).

45. Kato, T. et al. Temperature and biomass influences on interannual changes in CO2 exchange in an alpine meadow on the Qinghai-Tibetan Plateau. *Global Change Biology* **12**, 1285–1298 (2006).

46. Anthoni, P. et al. Forest and agricultural land-use-dependent CO2 exchange in Thuringia, Germany. *Global Change Biology* **10**, 2005–2019 (2004).

47. Gilmanov, T. et al. Winter CO2 fluxes above sagebrush-steppe ecosystems in

Idaho and Oregon. *Agricultural and Forest Meteorology* **126**, 73–88 (2004).

48. Marcolla, B. & Cescatti, A. Experimental analysis of flux footprint for varying stability conditions in an alpine meadow. *Agricultural and Forest Meteorology* **135**, 291–301 (2005).

49. Jacobs, C.M.J. et al. Variability of annual CO2 exchange from Dutch grasslands. *Biogeosciences* **4**, 803–816 (2007).

50. Fischer, M.L., Billesbach, D.P., Berry, J.A., Riley, W.J. & Torn, M.S. Spatiotemporal variations in growing season exchanges of CO2, H2O, and sensible heat in agricultural fields of the Southern Great Plains. *Earth Interact* **11**, – (2007).

51. Allison, V., Miller, R., Jastrow, J., Matamala, R. & Zak, D. Changes in soil microbial community structure in a tallgrass prairie chronosequence. *Soil Science Society of America Journal* **69**, 1412–1421 (2005).

52. Scott, R.L., Jenerette, G.D., Potts, D.L. & Huxman, T.E. Effects of seasonal drought on net carbon dioxide exchange from a woody-plant-encroached semiarid grassland. *J Geophys Res-Biogeo* **114**, (2009).

53. Saleska, S. et al. Carbon in amazon forests: Unexpected seasonal fluxes and disturbance-induced losses. *Science* **302**, 1554–1557 (2003).

54. Wilson, K. & Baldocchi, D. Comparing independent estimates of carbon dioxide exchange over 5 years at a deciduous forest in the southeastern United States. *J Geophys Res-Atmos* **106**, 34167–34178 (2001).

55. Bond-Lamberty, B. & Thomson, A. Temperature-associated increases in the global soil respiration record. *Nature* **464**, 579–U132 (2010).

56. Legates, D.R. & Willmott, C.J. Mean seasonal and spatial variability in global surface air temperature. *Theoretical and Applied Climatology* **41**, 11–21

(1990).

57. WIllmott, C. & Matsuura, K. Smart interpolation of annually averaged air-temperature in the United-States. *Journal of Applied Meteorology* **34**, 2577–2586 (1995).

58. Hopkinson, C., Jr & Smith, E. Estuarine respiration: an overview of benthic, pelagic and whole system respiration. *Respiration in Aquatic Ecosystems* (2005).

59. Caffrey, J. Factors controlling net ecosystem metabolism in US estuaries. *Estuaries* **27**, 90–101 (2004).

60. Solomon, C.T., Bruesewitz, D.A., Richardson, D.C., Rose, K.C., Van de Bogert, M.C., Hanson, P.C., Kratz, T.K., Larget, B., Adrian, R., Babin, B., Chiu, C.Y., de Eyto, E., Driscoll, C., Hamilton, D., Gaiser, E., Hendricks, S., Istvanovics, V., Laas, A., Pace, M., Staehr, P., Torgersen, T., Vanni, M. Weathers, K., & Zhu. G. Open water community respiration and primary production: drivers of daily variability in GLEON lakes around the globe. *Unpublished.*

61. Gudasz, C. et al. Temperature-controlled organic carbon mineralization in lake sediments. *Nature* **466**, 478–481 (2010).

62. Robinson, C. Heterotrophic bacterial respiration. *Microbial Ecology of the Oceans, Second Edition* (ed D. L. Kirchman), John Wiley & Sons, Inc., Hoboken, NJ, USA. (2008).

63. Rivkin, R. & Legendre, L. Biogenic carbon cycling in the upper ocean: Effects of microbial respiration. *Science* **291**, 2398–2400 (2001).

64. Alonso-Sáez, L. et al. Large-scale variability in surface bacterial carbon demand and growth efficiency in the subtropical northeast Atlantic Ocean.

Limnol. Oceangr. **52**, 533–546 (2007).

65. Allen, A.P., Gillooly, J.F., & Brown, J.H. Linking the global carbon cycle to individual metabolism. *Functional Ecology* **19**, 202–213 (2005).

66. Gillooly, J.F., Brown, J.F., West, G.B., Savage, V.M. & Charnov, E.L. Effects of Size and Temperature on Metabolic Rate. *Science* **293**, 2248–2251 (2001).

67. Kolokotrones, T., Van Savage, Deeds, E.J. & Fontana, W. Curvature in metabolic scaling. *Nature* **464**, 753–756 (2010).

68. DeLong, J.P., Okie, J.G., Moses, M.E., Sibly, R.M. & Brown, J.H. Shifts in metabolic scaling, production, and efficiency across major evolutionary transitions of life. *Proceedings of the National Academy of Sciences* **107**, 12941–12945 (2010).

69. Boltzmann, L. *Weitere studien über das wärmegleichgewicht unter gasmolekülen*. (1872).

70. Davidson, E.A. & Janssens, I.A. Temperature sensitivity of soil carbon decomposition and feedbacks to climate change. *Nature* **440**, 165–173 (2006).

71. Atkin, O. & Tojelker, M.G. Thermal acclimation and the dynamic response of plant respiration to temperature. *Trends in Plant Science* **8**, 343–351 (2003).

72. Gillooly, J. et al. Response to Clarke and Fraser: effects of temperature on metabolic rate. *Functional Ecology* **20**, 400–404 (2006).

73. Tjoelker, M.G., Oleksyn, J. & Reich, P.B. Modelling respiration of vegetation: evidence for a general temperature-dependent Q10. *Global Change Biology* **7**, 223–230 (2001).

74. Allen, A.P. & Gillooly, J.F. Towards an integration of ecological stoichiometry and the metabolic theory of ecology to better understand nutrient cycling. *Ecology Letters* **12**, 369–384 (2009).

75. Yvon-Durocher, G., Allen, A.P., Montoya, J.M., Trimmer, M. & Woodward, G. The Temperature Dependence of the Carbon Cycle in Aquatic Ecosystems. *Adv Ecol Res* **43**, 267–313 (2010).

76. Lopez-Urrutia, A., San Martin, E., Harris, R.P. & Irigoien, X. Scaling the metabolic balance of the oceans. *P Natl Acad Sci Usa* **103**, 8739–8744 (2006).

77. Niklas, K. & Enquist, B. Invariant scaling relationships for interspecific plant biomass production rates and body size. *P Natl Acad Sci Usa* **98**, 2922–2927 (2001).

78. Farquhar, G. & Caemmerer, S. A biochemical model of photosynthetic CO 2 assimilation in leaves of C 3 species. *Planta* (1980).

79. Bissinger, J.E., Montagnes, D.J.S., Sharples, J. & Atkinson, D. Predicting marine phytoplankton maximum growth rates from temperature: Improving on the Eppley curve using quantile regression. *Limnol. Oceangr.* **53**, 487–493 (2008).

80. Dewar, R., Medlyn, B. & McMurtrie, R. Acclimation of the respiration photosynthesis ratio to temperature: insights from a model. *Global Change Biology* **5**, 615–622 (1999).

81. Gifford, R.M. Plant respiration in productivity models: conceptualisation, representation and issues for global terrestrial carbon-cycle research. *Functional Plant Biol.* **30**, 171 (2003).

82. Bolker, B.M. et al. Generalized linear mixed models: a practical guide for ecology and evolution. *Trends in Ecology & Evolution* **24**, 127–135 (2009).

83. R Development Core Team R: a language and environment for statistical computing, Vienna, Austria. ISBN 3-900051-07-0 <http://http://www.R-project.org> (2011)

84. Zuur, A., Ieno, E., Walker, N. & Saveliev, A. *Mixed effects models and extensions in ecology with R*. (Springer Verlag: New York, 2009).

85. Pinheiro, J. & Bates, D.M. *Mixed-effects models in S and S-PLUS*. (Springer Verlag: New York, 2000).

86. Savage, V.H. Improved approximations to scaling relationships for species, populations, and ecosystems across latitudinal and elevational gradients. *Journal of Theoretical Biology* **227**, 525–534 (2004).

87. Enquist, B.J. Forest annual carbon cost: comment. *Ecology* **92**, 1994–1998 (2011).

88. Forsythe, W., Rykiel, E., Stahl, R., Wu, H. & Schoolfield, R. A model comparison for daylength as a function of latitude and day of the year. *Ecological Modelling* **80**, 87–95 (1995).

89. Chen, A. et al. Forest annual carbon cost: reply. *Ecology* **92**, 1998–2002 (2011).